remote sensing

MDPI

Article

An Investigation into Ground Movement on the Ventnor Landslide Complex, UK Using Persistent Scatterer Interferometry

William O'Connor [1], Gosia Mider [2,*], James A. Lawrence [2], Stewart Agar [2], Philippa J. Mason [3], Richard Ghail [4] and Jennifer Scoular [5]

[1] ByrneLooby Partners (Irl) Ltd., D12 VW27 Dublin, Ireland; WOConnor@ByrneLooby.com
[2] Department of Civil and Environmental Engineering, Imperial College London, London SW7 2AZ, UK; j.lawrence@imperial.ac.uk (J.A.L.); s.agar16@imperial.ac.uk (S.A.)
[3] Department of Earth Science and Engineering, Imperial College London, London SW7 2AZ, UK; p.j.mason@imperial.ac.uk
[4] Department of Earth Sciences, Royal Holloway, University of London, Egham TW20 0EX, UK; richard.ghail@rhul.ac.uk
[5] SkyGeo, Oude Delft 175, 2611 HB Delft, The Netherlands; jennifer.scoular@skygeo.com
* Correspondence: malgorzata.mider16@imperial.ac.uk

Abstract: Analysis of ground movement rates along the coastline and upper sections of the Ventnor landslide complex was carried out utilizing Persistent Scatterer Interferometric Synthetic Aperture Radar methods using Sentinel-1 SAR data from 2015 to 2019 (four years). Results were compared with rainfall data, historical ground investigation records and monitoring surveys carried out at Ventnor to relate observations to geology, geomorphology and rainfall. Decomposition of InSAR viewing geometries to vertical and horizontal aligned well with previous ground-based studies. Subsidence of -9.8 mm a^{-1} at the Lowtherville Graben and heave of +8.5 mm a^{-1} along the coastline south of Ventnor Park were observed. Decomposition to east-west geometry results showed an eastward displacement of approximately 12.4 mm a^{-1} along the coastline south of Ventnor Park, and a westward displacement of -3.7 mm a^{-1} throughout built up sections of Ventnor town, indicating the landslide was displacing more in an eastern direction than vertically. The cause of this movement was investigated by using publicly available intrusive boreholes paired with Persistent Scatterer Interferometry, and a new ground model spanning east-west parallel to the coastline was presented. No evidence of significant ground movement was observed along heavily protected sections of the coastline, suggesting coastal defences comprised of concrete aprons and rip rap appear to be an effective coastal management/landslide stabilisation tool when compared to rip rap alone. The mechanism of this increased stability is likely due to the combination of toe weighting and reduced toe erosion. A lag of approximately 13–20 days was observed between high rainfall events and subsequent peaks in ground displacement, which was shorter than a 29 day lag observed in a previous study. Similar observations of prolonged rainfall resulting in prolonged displacements were also observed. The study demonstrates the capabilities of the PSI methodology in identifying the same ground movements that conventional methods provide. By providing detailed analysis of ground deformation of the Ventnor landslide, we demonstrate small ground movements, validated with existing ground movement surveys. Similar methodology can be applied to coastal landslides in urban environments worldwide, providing a relatively cheap and rapid resource for coastal landslide monitoring.

Keywords: InSAR; coastal monitoring; persistent scatterer interferometry; landslides; earth observation; coastal processes; coastal engineering

check for updates

Citation: O'Connor, W.; Mider, G.; Lawrence, J.A.; Agar, S.; Mason, P.J.; Ghail, R.; Scoular, J. An Investigation into Ground Movement on the Ventnor Landslide Complex, UK Using Persistent Scatterer Interferometry. *Remote Sens.* **2021**, *13*, 3711. https://doi.org/10.3390/rs13183711

Academic Editors: Fabio Matano, Guido Ventura and Alberto Refice

Received: 12 July 2021
Accepted: 13 September 2021
Published: 16 September 2021

Publisher's Note: MDPI stays neutral with regard to jurisdictional claims in published maps and institutional affiliations.

Copyright: © 2021 by the authors. Licensee MDPI, Basel, Switzerland. This article is an open access article distributed under the terms and conditions of the Creative Commons Attribution (CC BY) license (https://creativecommons.org/licenses/by/4.0/).

1. Introduction

Coastal instabilities are an ongoing problem worldwide, occurring in various climates, topography, and geological formations. It was estimated that approximately 28,000 km^2 of coastline worldwide (excluding polar regions) were eroded between 1984–2015, twice that of land area gained during the same period [1]. In Europe, approximately 20,000 km of coastline was classified as being at risk of coastal erosion in 2004, which has likely increased and will continue to do so with rising sea levels and climate change [2]. On a regional scale in the United Kingdom, the southern coastline is susceptible to ongoing movement and erosion; well documented examples include Folkstone Warren due to the impact on the railway and the urban chalk coast of East Sussex [3–5]. The focus of this research is the town of Ventnor on the Isle of Wight, which was built on a slope which dips down to the coast and was subject to ongoing movement in recent years [6].

A review of coastal erosion rates was carried out in 2010 as part of the Shoreline Management Plan 2 [7], and estimates of future rates were made. For Ventnor Bay, estimates ranged from 0.46 m a^{-1} for the period 2010–2025 and 0.77 m a^{-1} for 2085–2105. It is to be noted that these estimates account for the life span of existing costal defences, and their potential deterioration due to ongoing erosion. Such deterioration may result in exacerbated ground movements along the coastline over time.

Interferometric synthetic aperture radar (InSAR) is a remote sensing technique which uses the phase difference between two synthetic aperture radar (SAR) images obtained from an orbiting antenna to determine displacement in the line of sight (LOS). Displacement of a measurable feature (scatterer) in the images will affect the distance and timing of the backscattered signal being measured, and subsequently produce a measurable change in the SAR signal phase between images [8]. SAR scenes used in this study were obtained from Sentinel-1A and Sentinel-1B satellites, launched as part of the Sentinel-1 mission by the European Space Agency (ESA). The satellites are orbiting along the same trajectory but in opposing orbits (separated by 180°), with a revisit time for a given location of 12 days per satellite, equating to approximately 6 days for 2 satellites. This study utilized the Interferometric Wide swath imaging mode, which typically measures an area of 250 km with a 5 × 20 m spatial resolution [9]. The frequent repeat time, wide area of coverage and open access to data allows for inexpensive, long-term monitoring of ground deformation. Applications of InSAR include monitoring natural and human induced ground deformation from a range of activities including dewatering [10], inland landslide movements [11–14], land usage [15] and coastal geomorphological processes [16]. InSAR monitoring is best applied to slow deformation rates (1 mm a^{-1} < Velocity < 0.8 m a^{-1}, considering Sentinel 1 specifications) [12–14]. Interferometric methods are generally limited in measuring rapid deformations owing to the nature of the observations i.e., gathering mean velocity by unwrapping phases for the time period between satellite visits. This limitation is discussed in detail by e.g., Crosetto et al. [17]. However, the limitation can be overcome by means of complementing SAR methods with Digital Image Correlation [18] or Offset-Tracking [19].

Monitoring of coastal retreat and ground movement in coastal locations can be difficult, due to factors such as safety, cost, and methods used. Traditionally, coastlines have been mapped manually in field surveys which are prone to error, induce safety risks, are labour intensive, as well as being infrequent. With the advent of aerial imagery, a new asset management tool was available to cartographers, providing large spatial datasets which could be regularly repeated [8]. However, these too are prone to errors relating to parameters such as flight-path geometry, cloud cover over locations and they are extremely costly. Such imagery can be used to determine coastal erosion rates over long periods of time, and hence processes causing erosion can be identified when paired with other monitoring techniques [20]. More recently, surveys have utilized global positioning systems (GPS) to accurately map coastlines either as point data collected in the field by a receiver, or as imagery and photogrammetry [21]. Further developments in remote sensing include Light Detection and Ranging (LiDAR), which exploits ranges recorded from pulsed lasers from an aerial vehicle flight-path, can measure displacements at points

by use of elevation data, and can help to understand processes leading to instability [22]. The aim of this study is to monitor coastal erosion and landslide processes using Persistent Scatterer Interferometry (PSI) by analysing a coastal chalk landslide complex at Ventnor to establish its effectiveness as a landslide and coastal defence management monitoring tool, and to assess whether PSI can be used to quantify and interpret ongoing natural geological processes.

While PSI was applied for analysis for several decades, the majority of research relating to landslides has been focused on land-locked landslides [11–14]. These studies also paired InSAR data with data from other monitoring methods (i.e., GPS, corner reflectors to increase PS generation boreholes with inclinometers and piezometers). Additionally, data from Sentinel-1A and 1B satellites have only been available from 2014 onwards. The orbit and frequent revisit time (6 days) provide better coverage when compared with previous studies by Yin et al. [11], who utilised data from the RADARSAT, which had a revisit time of 24 days. Other studies such as Polcari et al. [10] and Ciampalani et al. [12] utilised data from COSMO-SkyMed, which is somewhat expensive to acquire, whereas data from Sentinel missions are available for free. While InSAR methods have been used to monitor coastal regions, no study has focused specifically on coastal landslides. Sajinkumar et al. [16] discuss the use of PSI for assessing changes in beach morphology, and Polcari et al. [10] used InSAR to monitor natural and anthropogenic ground deformation along coastal regions in Italy, however did not monitor any coastal landslides. The Ventnor Undercliff landslide is considered the largest urbanised coastal landslide complex in England and Wales and one of the largest in north-west Europe [7]. It is, however not the only coastal landslide located within an urban area, therefore the analysis and monitoring methods utilised in this study can be used on any urban coastal landslide, providing relatively quick and cheap monitoring options.

2. Study Region

2.1. Overview and Bedrock Geology

The focus of this project is the town of Ventnor (SZ 55,944 77388), on the southern coastline of the Isle of Wight, United Kingdom. The Isle of Wight is located in the English Channel, between 3 and 8 km from the Hampshire coast mainland. The location of the Isle of Wight in relation to Great Britain is shown in Figure 1a, with the location of Ventnor also shown in relation to the Isle of Wight in Figure 1b. From a geological perspective the Isle of Wight forms part of the Hampshire Basin, which consists of Cretaceous and Paleogene age sedimentary rocks. The southern half of the island consists of Cretaceous outcrops of chalk, limestone, mudstone, sandstone, and siltstone [23,24].

The town of Ventnor overlies a large landslide complex known as the Undercliff, which spans approximately 8 km of the southern coastline from St. Catherine's in the west to Ventnor in the east, shown in Figure 2a. The majority of development in the town is on a steep incline from +5 m Ordnance Datum (OD) at Ventnor beach to +102.6 mOD at Ocean View Rd. Ventnor is known to be undergoing slow, constant seaward ground movement with records dating back to the early 1800's and continuing to the current day [6].

Bedrock geology underlying Ventnor consists of Grey Chalk, Upper Greensand, Gault Clay and Sandrock, as shown in Figure 2a. The three boreholes [25] indicated on this map align approximately with the ground model developed by Halcrow in 2006 [26], shown in Figure 2b. The ground model identifies two distinct sections to the landslide. The upper section spans from Newport Road to Park Avenue, and the lower section from Park Avenue to the shoreline. The basal failure surface in the upper section is in the interface between the Gault Clay and Monk's Bay Sandstone (formerly known as Carstone), approximately +5 mOD. This section is well defined locally as the Lowtherville Graben, located south of Ventnor Golf Club (grid reference SZ 54675 77761). The lower section is less well defined, with ongoing back-tilting of blocks of chalk debris, Upper Greensand and Gault Clay overlying Monk's Bay Sandstone and Sandrock, resulting in movement from Ventnor Park to the beach. The failure surface is at approximately −10 mOD in the Lower Greensand. The

upper section contributes to heave along the crest of the lower section, and both sections are basal non-circular rotational. Strata descriptions given below are based on information obtained from the British Geological Survey (BGS) Lexicon of Named Rock Units [27].

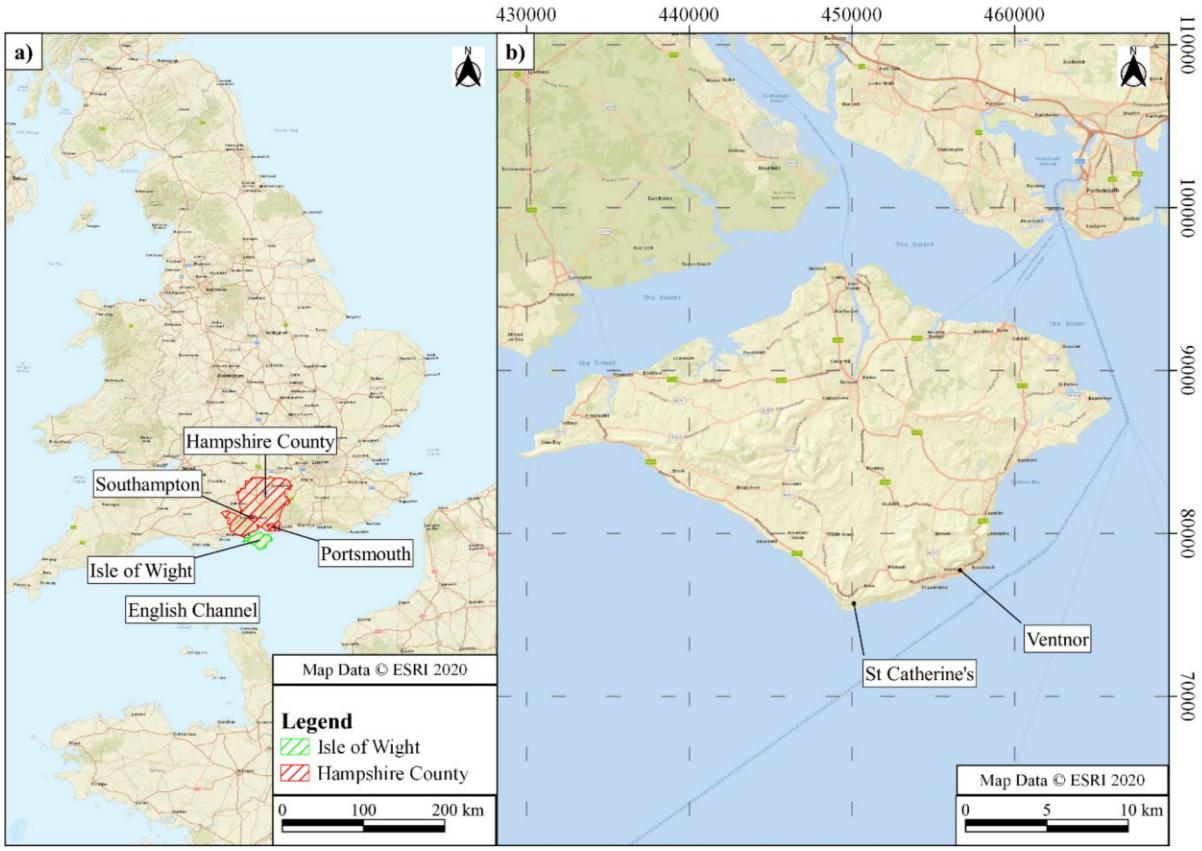


Figure 1. Location of the Isle of Wight in relation to Great Britain (**a**) and the location of Ventnor on the Isle of Wight (**b**). Image created on QGIS with background imagery from ESRI World Street Map (Service Layer Credits: Esri, DeLorme, HERE, USGS, Intermap, iPC, NRCAN, Esri Japan, METI, Esri China (Hong Kong), Esri (Thailand), MapmyIndia, Tomtom).

- Gault formation—A mudstone containing laminae of fine-grained sand and silt, with some micaceous, shelly, phosphatic nodules.
- Upper Greensand formation—Generally described as fine-grained sand and sandstone, finely interbedded with glauconitic layers, resulting in weak to strong cementation. The beds can be split into upper beds, comprised of cherty sandstone, and lower beds described as the Passage Beds.
- Monk's Bay Sandstone formation (Formerly known as Carstone)—A sandstone containing medium to coarse grains with some pebbly seams. Seams are ferruginous and micaceous.
- Sandrock formation—A weakly cemented sandstone comprised of medium-grained quartz sand. Thin, grey, micaceous mud laminae can be found mainly at the base.
- Grey Chalk debris—Grey Chalk formations encountered include Zig Zag Chalk and West Melbury Marly Chalk, characterized by their thin bedding, marly composition and off white to grey colour.

2.2. Historical Movement and Previous Monitoring Surveys at Ventnor

Historical records indicate ground movement occurred at Ventnor since at least the early 1800's, a summary of which is given in Chandler [28]. Significant movements occurred between 1960 and 1961, including a seven-day period where movements were as large as 19 mm per day at Bath Road. This was related to extremely large rainfall events, where

annual total rainfall in 1960 was 1355 mm, compared to 840 mm on average for the previous 57 years. This resulted in development of fissures, and damage to buildings, roads, and utilities. Subsidence was recorded at Steephill Down Road, located at the crest of the upper section of the landslide, and heave occurred along the foreshore. Slow, intermittent movements have been recorded since, with those in the period 1963–1981 occurring in years with above average rainfall.

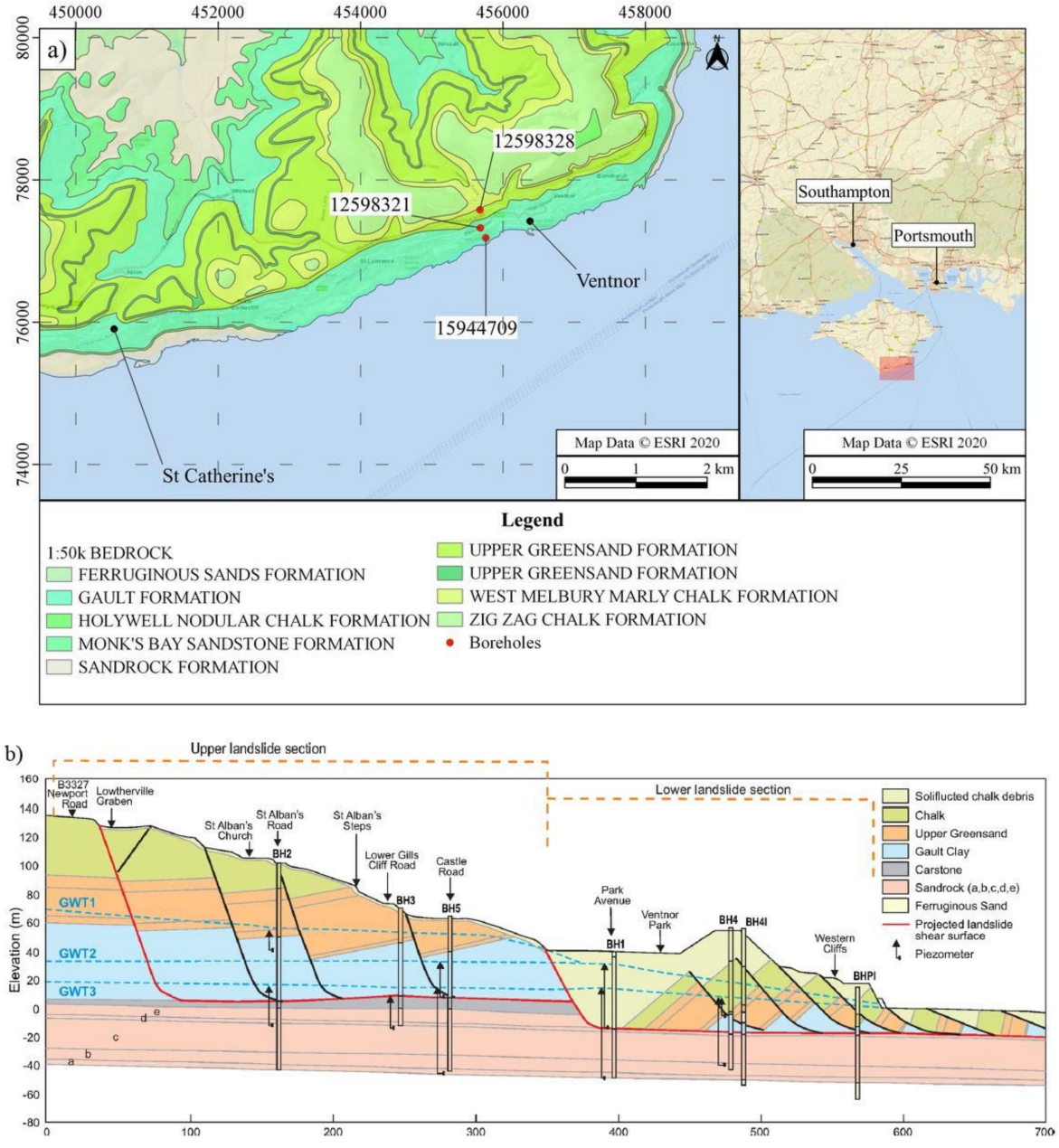


Figure 2. Study area map with BGS 1:50,000 bedrock geology map overlain, with 3 borehole records obtained from the BGS online portal indicated in red with reference number also given [25] (**a**). Ground model developed by Halcrow [26] approximately in line with 3 boreholes in (**a**) showing postulated failure surfaces (**b**). Upper landslide section extends from Newport Road to approximately Park Avenue. Lower section extends from north of Park Avenue beyond the Western Cliffs and into the sea bed. The bedrock geology map of Isle of Wight was accessed via the EDINA DigiMap service, using data provided by BGS last updated in 2013, plotted on QGIS with background imagery from the ESRI World Street Map (Service Layer Credits: Esri, DeLorme, HERE, USGS, Intermap, iPC, NRCAN, Esri Japan, METI, Esri China (Hong Kong), Esri (Thailand), MapmyIndia, Tomtom).

Numerous studies have been undertaken to determine ground movements on the Ventnor landslide. Chandler [28] implemented a one-year field survey using various methods to record vertical and horizontal (perpendicular to the coastline) movements in selected areas of Ventnor, summarised in Table 1. Average rates for the Lowtherville Graben section were 20–25 mm a^{-1} subsidence and 20 mm a^{-1} seawards (perpendicular to the coastline). Geomorphological Services Limited compiled records from various surveys carried out pre-1991, which compromised benchmark, ground-based and photogrammetric surveys, summarised in Table 1 [29]. It is worth noting the general trend in estimates of annual ground movement rates decreased with longer monitoring periods, as extreme events were smoothed out by years in which little to no movement was observed.

Table 1. Historical monitoring surveys at Ventnor, after Chandler [28], Geomorphological Services Limited [29], Moore et al. [30].

Survey Method	Location	Monitoring Period	Estimated Annual Rate of Vertical Movement (mm a^{-1})
Benchmark Survey	Steephill Down Rd	1960–1982	29
	Newport Rd	1960–1982	28
	Albert St	1939–1960	27
	Gills Cliff Rd	1939–1982	19
	Ocean View Rd	1939–1982	12
	Bath Rd	1907–1982	11
Extensometer Survey	Newport Rd	1981–1982	20 to 39
	Havenbush	1981–1982	27 to 30
	Gills Cliff Rd	1981–1982	16
Ground Survey	Newport Rd	1988	12 to 125
	Winter Gardens	1988	30
Photogrammetry	Ocean View Rd	1949–1988	67
	Bath Rd	1949–1988	65
	Esplanade	1949–1988	20
	Belle Vue Rd	1949–1988	15
Council Records	Bath Rd	1995–2005	33
	Newport Rd	1995–2005	22

A range of automatic monitoring equipment was installed since 1992, including vibrating wire piezometers at Winter Gardens, crackmeters and settlement cells at the Lowtherville Graben, and a weather station at Ventnor Park [31]. Further installations in 2002 and 2005 consisted of piezometers and inclinometers at St Alban's Road to a depth of 93 mBGL and Ventnor Park to a depth of 76 mBGL, to assess the deep seated nature of the landslide, as shown in Figure 2b. The approximate locations of installations from both surveys are presented in Figure 3a. Furthermore, 50 permanent ground markers were installed throughout the Ventnor area and measured using GPS survey equipment after one year, as detailed in Moore et al. [30]. No detectable movement was observed over this time period. The same study reviewed council records between 1995 and 2005 for Bath Road and Newport Road, which indicated subsidence of 33.2 and 22 mm a^{-1}, respectively. Carey et al. [32] identified a lag between high rainfall events and pore pressure generation, where a response was recorded after 7 days, however it took approximately 29 days to reach a peak, which then lasted approximately 30 days. The highest rainfall events did not yield the largest displacement responses, rather prolonged rainfall periods led to a higher generation of pore pressures, resulting in larger displacements.

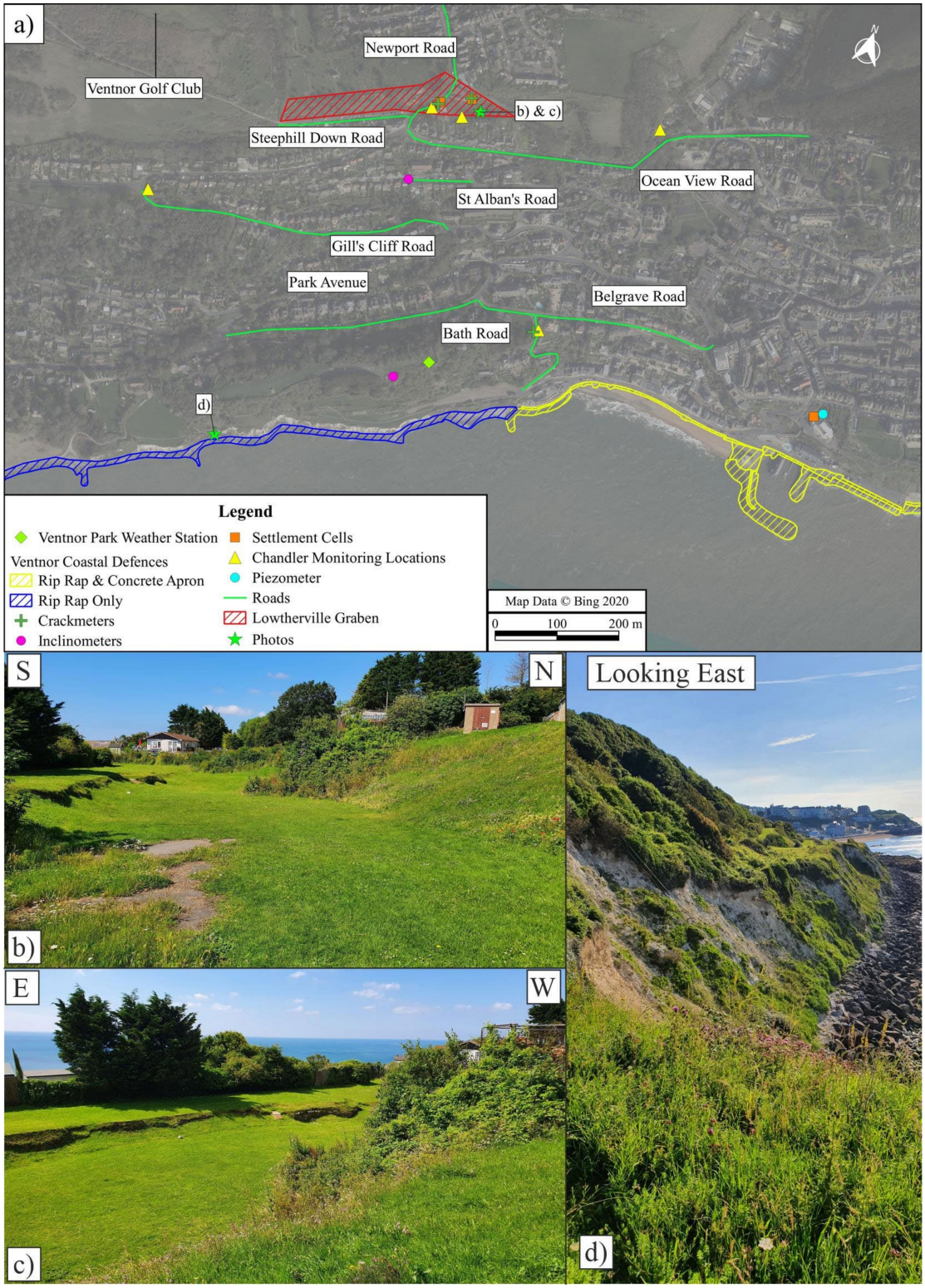


Figure 3. (**a**–**d**): Instrumentation locations at Ventnor, after Chandler [28], Geomorphological Services Limited [29], and Moore et al. [30] (**a**). Image shows the transition between rip rap and/or the concrete apron and rip rap only along the coastline. Image (**b**,**c**) shows ongoing movement at the Lowtherville Graben, showing settlement in the middle of the Graben that creates ca. 8 m tall berm to the north and 0.5 m to the south. Image (**d**) shows the toe of the landslide, with a rock apron present along the shoreline. The steep angle of the chalk cliff demonstrates the active erosion at the site. Image (**a**) created on QGIS with background imagery from Bing Maps (2020).

In March 2013, Newport Road was closed as a result of ground movement, requiring emergency repair works [33]. In January 2020, a section of wall collapsed along Belgrave Road, resulting in closure of the road [34]; more recently in January 2021 a slide occurred off Alpine Road where a large retaining wall partially failed, resulting in displacement of material [35]. While no numerical values are available for these recent events, and two lie outside the monitoring period of this study, it is clear movement is still ongoing. Therefore, recent very slow to slow movement is likely to have been recorded by InSAR monitoring, presented in the results and discussion.

A site walkover survey was completed in July 2021 to ascertain localised ground movements and different aspects of the landslide, shown as Figure 3. It was observed that settlement is occurring at the Lowtherville Graben, producing an approximately 8 m vertical berm to the north, and a 0.5 m exposed section of the graben which is not vegetated (see Figure 3b,c). The coastal defences in the form of a rock apron is seen in Figure 3d. While these do provide some protection to the toe, they appear shallow and the size of the rip rap do not appear significant enough to prevent overtopping and subsequent erosion of material behind the rock apron. Figure 3 also outlines the dense vegetation present throughout the landslide, and hence low PS generation.

3. Methods

3.1. Sentinel-1 Data Processing

PSI processing of Sentinel-1 SAR data was employed in this study. PSI is a specialized method of Differential InSAR (DInSAR) which identifies radar targets with high phase stability throughout the image time series [36]. In depth descriptions of PSI algorithms are covered in the literature [17,37]; the configuration used here utilised a single master configuration and pixel selection based on amplitude dispersion. Single look complex (SLC) images were retrieved from the Alaska Satellite Facility (ASF) Vertex service [38] for dates between 19 March 2015 and 29 December 2019 for ascending orbit, and 3 May 2015 to 22 August 2019 for the descending orbit. The relevant track identifier and number of scenes is outlined in Table 2 [9].

Table 2. SLC scene acquisitions, total number of scenes processed and processing software following comparison with tidal data from Portsmouth [9,39].

Orbit	Ascending	Descending
Track Number	132	81
Heading Azimuth (°)	344.89	188.26
Look Angle (°)	74.89	278.26
Total Number Scenes in Time Period	209	205
Number of Scenes Post Tidal Comparison	80	104
Number PS Points Generated	3262	3919

As this study focused on coastal locations, Sentinel-1A and Sentinel-1B scene acquisition times had to be compared with tidal data obtained from Portsmouth, the nearest tidal monitoring station [39], which had tidal peaks within 20 min of those at Ventnor. This was done to select scenes captured at low tide, when the platform/toe of the coastal defences were exposed, hence maximizing the number of PS generated. A buffer of one hour was allowed for either side of the recorded high tide time, and matching scenes were returned. The merits of this method were highlighted previously by Mider et al. [40]. The original number of scenes downloaded as part of the study, and the number remaining following comparison with tidal data are summarised in Table 2. Large gaps in suitable scenes for monitoring the ascending data were observed between 14 May 2018 and 4 March 2019 and between 21 May 2019 and 12 October 2019, where no scene was captured at low tide. The former was hindered by missing values in the dataset between 27 January 2019 and 14 February 2019.

PSI allows for precise measurements of interferometric phase and accurate calibration of error terms. It is expected that PS generators include corners of buildings, metal structures, and rough exposed rockfaces. PS generation on smooth surfaces, vegetated areas, and bodies of water is rare, as can be seen in Figures 4 and 5 where PS generation in Ventnor Park was low for both orbits, and PS generation was high throughout Ventnor town, where more development is present. The effects of noise on the accuracy of deformation results can be estimated via the temporal (or 'ensemble') coherence of the phase in a measurement time series. PSI processing removes any points that exhibit low coherence, as these will likely yield lower-accuracy results.

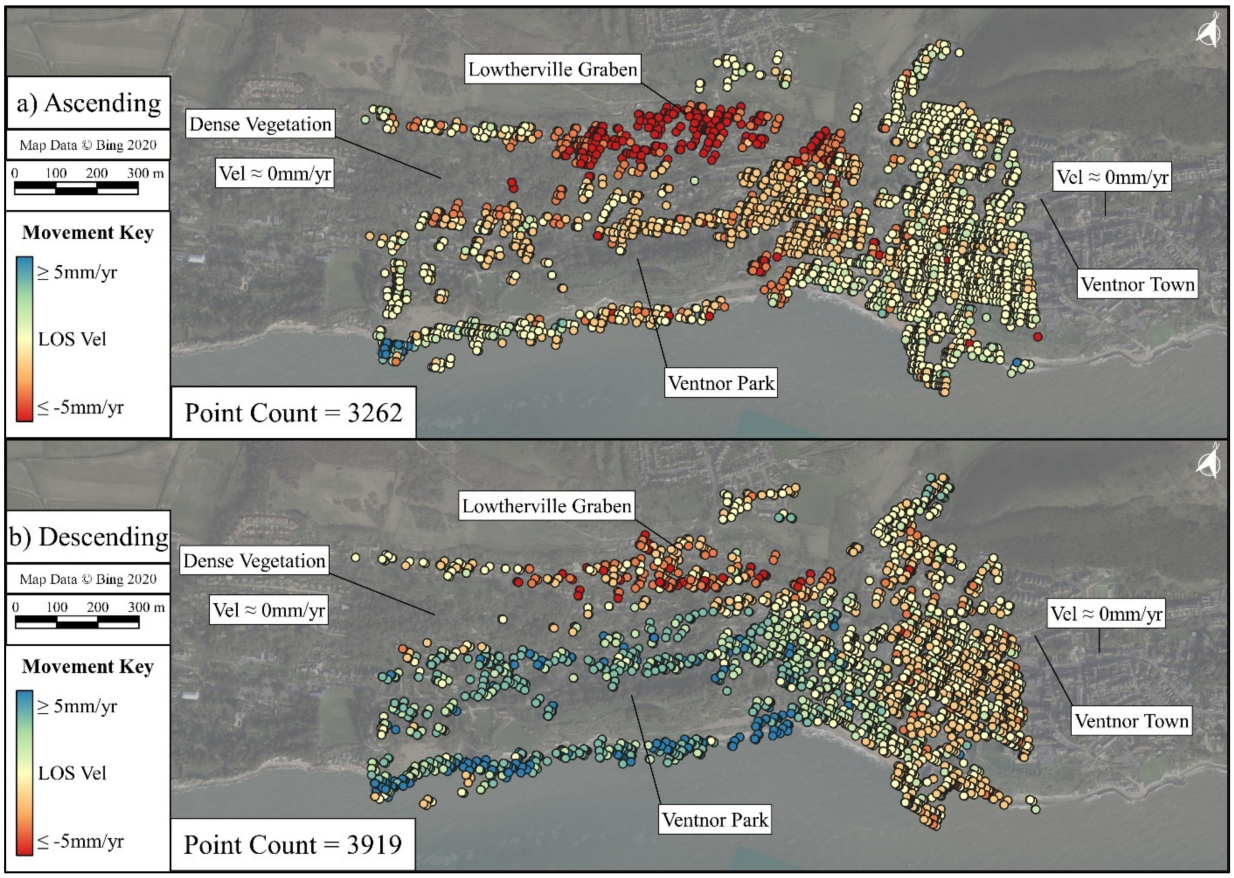


Figure 4. (**a**,**b**): Distribution of PS points generated from ascending (**a**) and descending (**b**) Sentinel 1 orbits for the Ventnor Scheme 2020.

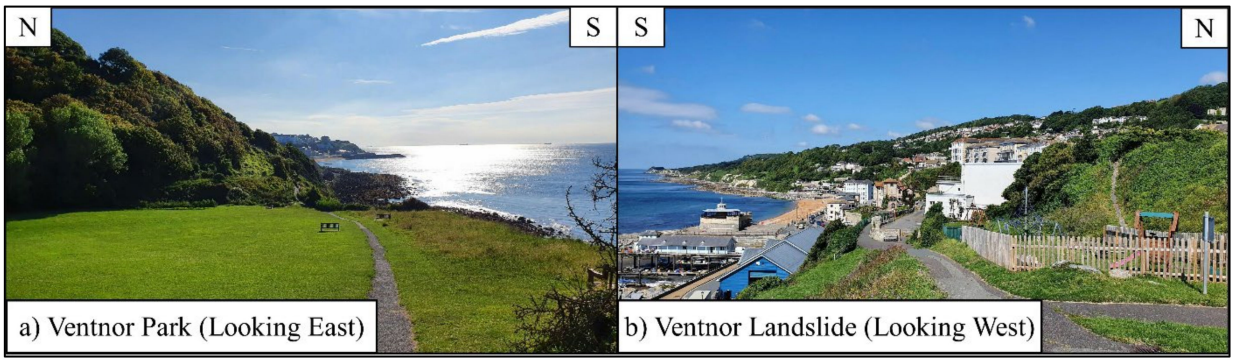


Figure 5. (**a**,**b**): Ventnor Park (**a**) where vegetation is present and hence a lack of PS generators. Image (**b**) shows the abundance of PS generators (houses, fences, walls etc.) resulting in the greater density of points toward the east as shown in Figure 4.

For this study the coherence threshold was set at 0.65 to allow a greater number of PS points to be observed, and thus a larger study area analysed. In total, 3262 PS points for the ascending orbit and 3919 PS points for the descending orbit were generated, as shown in Figure 4. It is noticeable that a greater number of PS points were generated for the descending orbit, which may be due to different sensing geometries (see Section 3.2), the greater number of post-tidal scenes processed in the descending set, or slight differences in processing methodology.

Average raster maps of scatterer velocity in the line of site (V_{LOS}, see Section 3.2) were created using the built in Inverse Distance Weighted (IDW) interpolation tool in QGIS. Following the approach from Raspini, Cigna and Moretti [41] the power was set to 2, the search radius was set to variable and the minimum number of points was set to 12. A seven-scene moving average was applied to smooth out the results when plotted to allow the user to interpret results more easily. Similarly, daily rainfall records obtained from the Ventnor Park rain gauge were plotted to investigate correlations between high rainfall periods and increases in ground movement rates [31]. As there are a minimum of six days between satellite passes there is an ambiguity as to when movements have occurred exactly within this interferometric measurement window. As such there is some ambiguity in linking particular rainfall events to a measured movement. All mapping is georeferenced to Ordnance Survey Great Britain Datum (OSGB36).

3.2. Obtaining Estimates of Vertical and Horizontal Velocity from InSAR

As previously mentioned, InSAR measures displacement and velocity in the LOS (D_{LOS} and V_{LOS}, respectively) of satellite viewing angle. While this provides a good initial indicator for ground movement, it can be misleading when trying to understand geomorphological processes. Therefore, true vertical and horizontal (east-west) values are preferable. Fuhrmann and Garthwaite [42] suggest the decomposition of LOS values by the use of opposite satellite viewing and orbital geometries. Landslide ground movement rates perpendicular to the coastline (and approximately parallel to N-S) have been extensively studied (see Section 2.2). Owing to difficulties in resolving the true component of N-S movement in Sentinel-1 data, the N-S element of movement has been neglected. The resulting Equation (1) was used to estimate vertical and E-W horizontal velocities, based on orbit geometries and sign conventions in Figure 6. Subscripts *a* and *d* denote ascending and descending, respectively. Subscripts *E* and *U* denote horizontal (east-west) and vertical, respectively. The matrix was solved for V_U and V_E, which were subsequently used as coefficients in the QGIS raster calculator, allowing for the previously generated IDW raster maps to be combined and allowing for the generation of indicative maps of vertical and horizontal displacement. Sign conventions for the respective measurements are presented in Table 3. For maps, a multispectral colour ramp was adapted where the limits are set symmetrically around 0 based on histogram data, i.e., $\geq$ +4 mm a^{-1} to ≤ -4 mm a^{-1} for a case where a large quantity of points are within the range +4 to −4. Any value greater than +4 mm a^{-1} is coloured blue, and any less than −4 mm a^{-1} is coloured red.

$$\begin{pmatrix} V_{ASC} \\ V_{DESC} \end{pmatrix} = \begin{pmatrix} -\sin\theta_a \cos\alpha_a & \cos\theta_a \\ -\sin\theta_d \cos\alpha_d & \cos\theta_d \end{pmatrix} \begin{pmatrix} V_E \\ V_U \end{pmatrix} \quad (1)$$

where:

V—Average velocity (mm a^{-1});
α—Orbit azimuth angle;
θ—Incidence/Look angle.

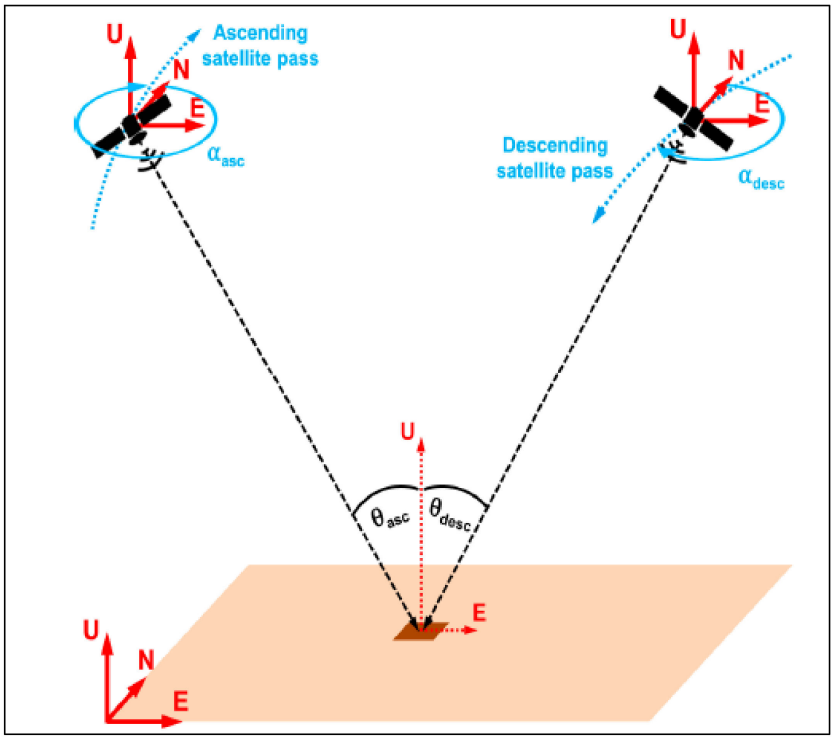


Figure 6. 3D InSAR geometry adapted from Fuhrmann and Garthwaite [42]. Sentinel 1 always looks to the right. Sign conventions are summarized in Table 3. In relation to Ventnor, the cliff spans east-west, and satellite passes are nearly perpendicular to the cliff.

Table 3. Sign conventions used for remote sensing. D denotes displacement measured in mm, and V denotes average velocity in mm a^{-1}. Conventions for V_U and V_E follow those adapted in Fuhrmann and Garthwaite [42]. The subscript LOS denotes in the line of sight, as discussed in Section 1.

Parameters	Direction (Value)	Colour
V_{LOS} and D_{LOS}	Away from satellite (−ve)	Red
V_{LOS} and D_{LOS}	Towards satellite (+ve)	Blue
V_U and V_E	Toward origin (−ve)	Red
V_U and V_E	Away from origin (+ve)	Blue

4. Results and Discussion

In this section, processed InSAR results are presented to determine ground movement rates and causes on the Ventnor landslide. Standard InSAR methodology as described in Sections 3.1 and 3.2 were followed, and average velocity/displacement maps were compared with time series plots D_{LOS} and daily rainfall records from the Ventnor Park rain gauge [31].

4.1. Results Verification

To enable a direct comparison with the one-year studies carried out by Chandler [28] and the Geomorphological Services Ltd. [29], a windowed sample of results for 2016 was assessed, as it had the greatest number of low-tide scenes for both ascending and descending orbits. PS with $V_{LOS} > 20$ mm a^{-1} and $V_{LOS} < -20$ mm a^{-1} for 2016 are shown in Figure 7. Clusters of subsidence occurred near Lowtherville Graben, and heave at Ventnor Park, as expected based on Figure 2b in Section 2.1 and previous in-situ monitoring surveys summarised in Table 1.

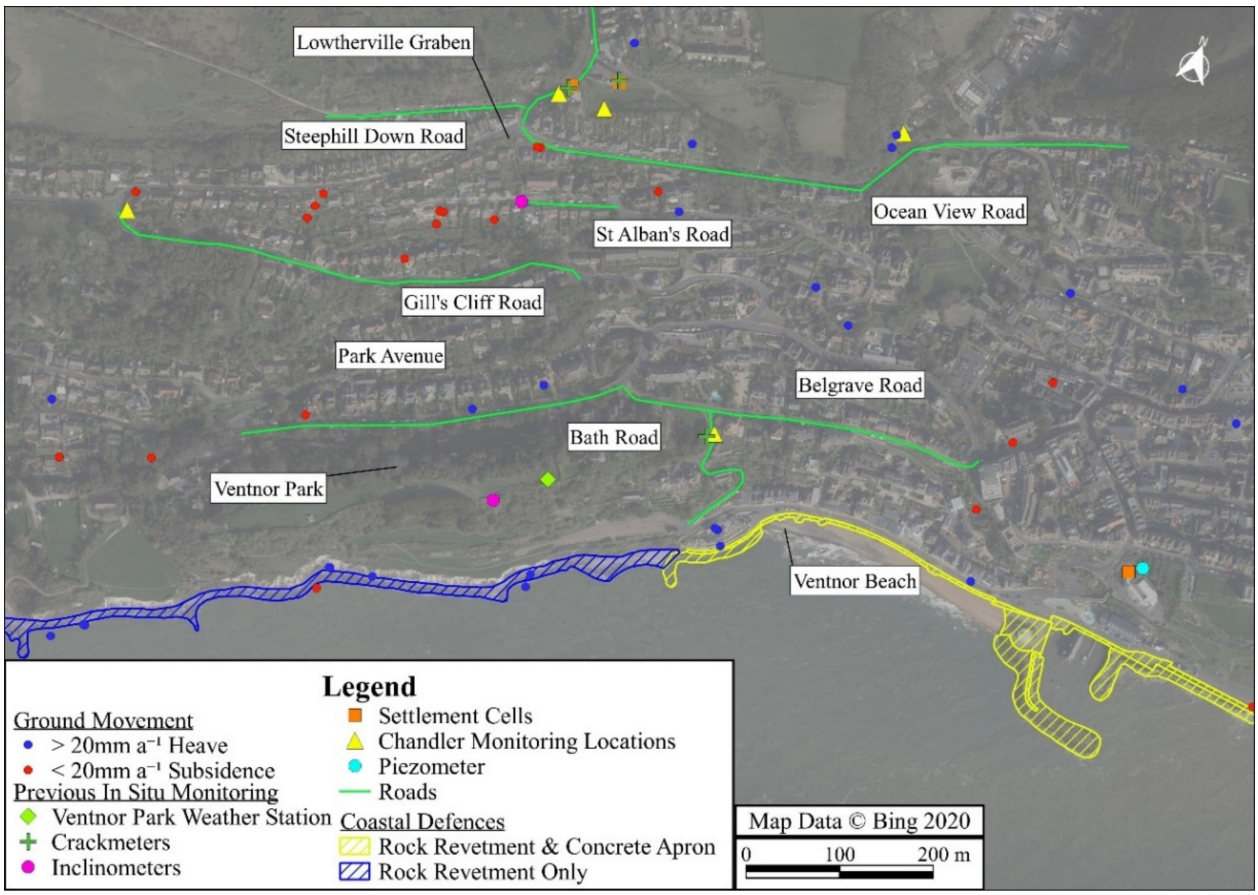


Figure 7. PS at Ventnor showing large heave/subsidence in both orbits ($V_{LOS} > 20$ mm a^{-1} and $V_{LOS} < -20$ mm a^{-1}) in 2016. The image was created on QGIS with background imagery from Bing Maps (2020).

While this gives an indication of point locations with high V_{LOS}, it is still not directly comparable to purely vertical measurements obtained during field surveys and does not offer insight into the overall trends occurring throughout the Ventnor landslide. Using the methods described in Section 3.2, estimates of V_U and V_E were obtained for a windowed sample of suitable scenes collected during 2016, as shown in Figure 8a,b.

It is seen that there is a significant E-W component to the landslide, which was not been captured in the ground model developed by Halcrow [26], previously presented in Figure 2b. To further investigate the nature of this movement, a 2D ground model was generated using BGS publicly available borehole records located west of Ventnor Park [25]. A failure surface inclined at approximately 3° to the horizontal and dipping to the east is recorded at 0 mOD in the Gault Clay and chalk debris, however no description of the shape is given. This failure surface is approximately drawn on the cross section in Figure 9, showing that the overlying block of material is sliding eastward along the postulated failure surface, while the underlying block of material remains static. A similar W-E component is observed throughout Ventnor town, however it is not as significant due to the presence of heavier defences spanning further east. It is likely both of these are second order movements caused by the more significant N-S sliding mechanism (not detected by InSAR due to sensing geometries) resulting in lateral spread. Qualitatively, the results aligned well with observations from InSAR data, showing that InSAR can be used to predict possible failure surfaces when paired with intrusive investigations. This served as a verification of results from InSAR, allowing the authors to proceed with analysis for the full time series. The true range of values for V_U was −18.7 to +30 mm a^{-1}, and V_E −16.9 to +14.5 mm a^{-1}, V_U being within the ranges presented in Table 4.

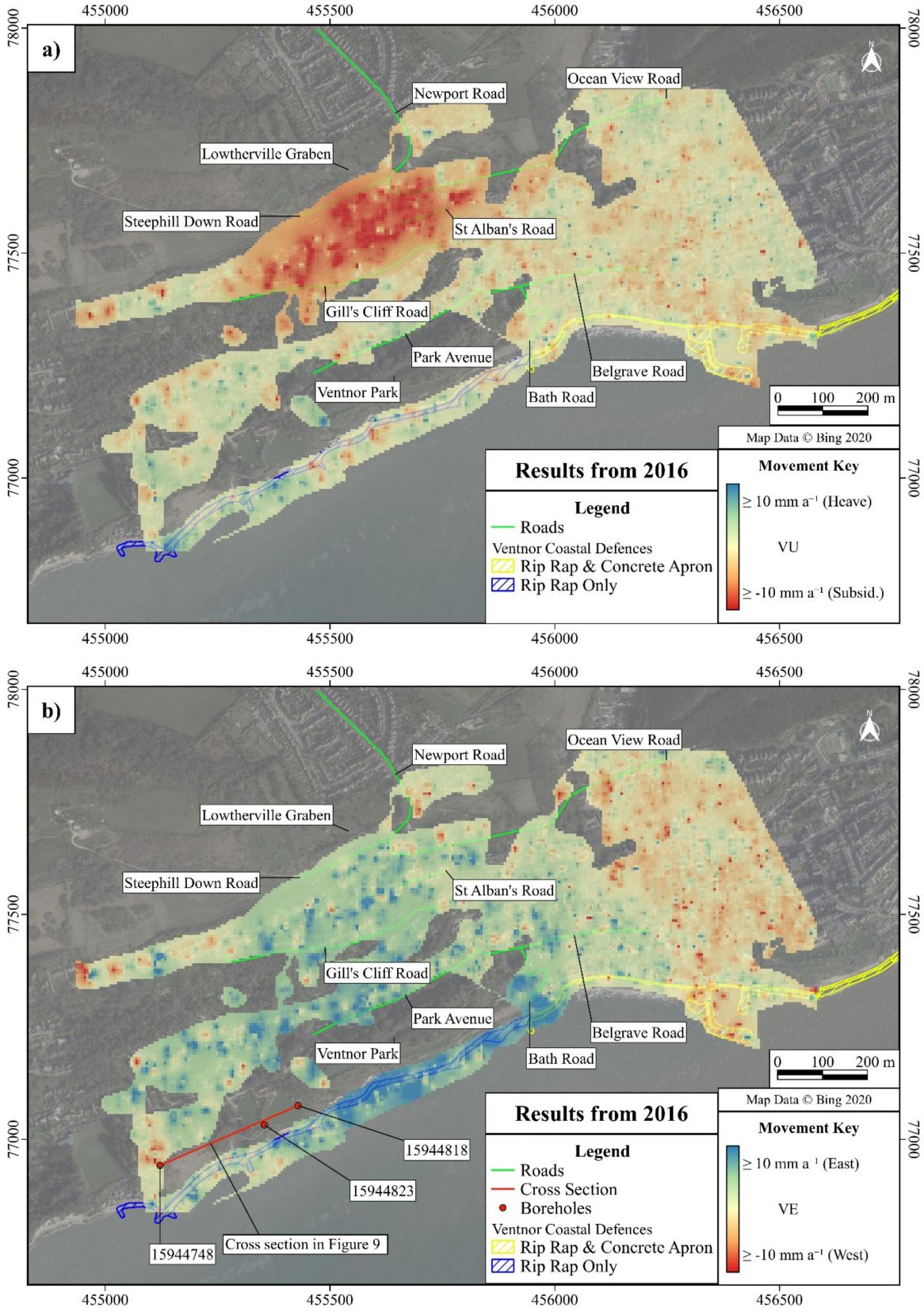


Figure 8. (**a**,**b**): Vertical velocity (V_U) component (**a**) and horizontal velocity (V_E) component (**b**). Suitable scenes captured during 2016 were used to generate images. Boreholes and approximate cross sections generated in Figure 9 are shown in red on (**b**). Images were created on QGIS with background imagery from Bing Maps (2020).

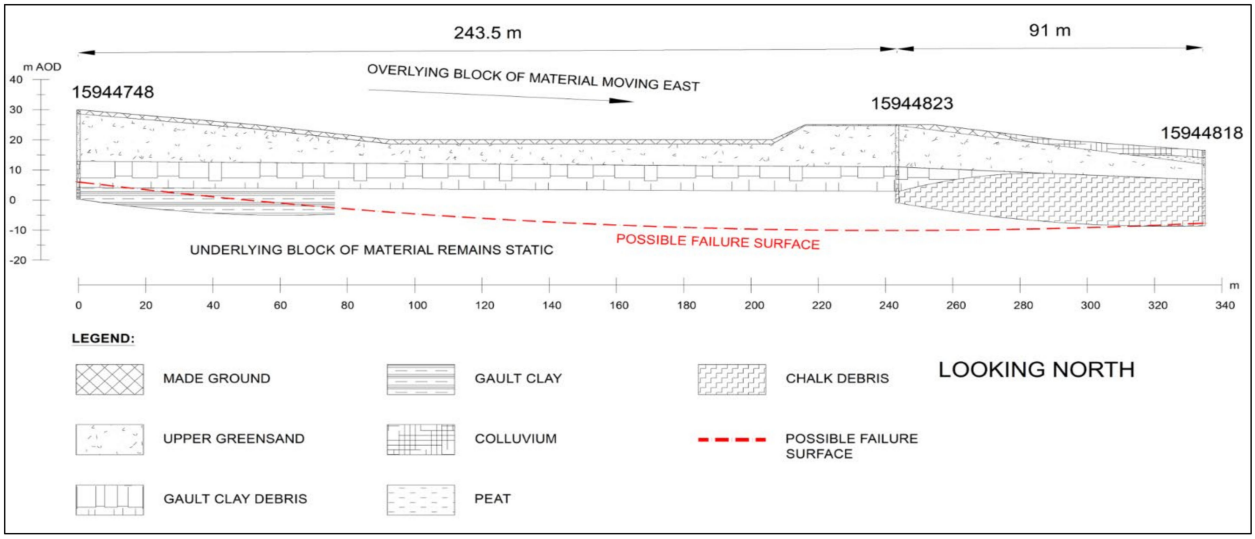


Figure 9. 2D E-W ground model spanning boreholes shown in Figure 8b to the west of Ventnor Park. Failure surface shown approximately 0 m OD dipping parallel with ground level in red is indicative; it is not known if this failure surface is planar or curviplanar. The mechanism consists of the overlying block of material sliding east along the failure surface in the Gault Clay/chalk debris, with the underlying block remaining static.

Table 4. Summary of min and max vertical (V_U) and horizontal (V_E) in Ventnor during 2016.

Time Series	Value	V_U (mm a^{-1})	V_E (mm a^{-1})
2016	Min (Subsidence/West)	−16.9	−18.7
	Max (Heave/East)	14.5	30

4.2. Full Time Series Analysis

For the full time period monitored by InSAR, March 2015 to December 2019 for ascending scenes and May 2015 to August 2019 for descending scenes, an IDW raster of V_{LOS} was created to check for long term movement trends. Results were paired with time series D_{LOS}, and rainfall records from the Ventnor Park rain gauge, plotted in Figures 10 and 11. The minimum, average and maximum D_{LOS} measurements for a selection of points (shown as subsets on Figures 10 and 11) were plotted as time series charts smoothed out using seven scene moving averages described in Section 3.1.

D_{LOS} values from ascending orbits suggest movement is not taking place at a constant rate, rather undergoing a cycle of increased displacement rates followed by a plateau, in particular at the Lowtherville Graben. These increased subsidence rates usually follow periods of above average rainfall, an example being prolonged rainfall from 10 December 2016 to 7 March 2017, a cumulative total of 244.4 mm, triggered subsidence of −1.5 mm at the Lowtherville Graben on 1 April 2017. This equates to a delay of 20 days (Figure 10b), shorter than the observation by Moore et al. [30]. Cumulative rainfall of 317.7 mm between 17 May 2017 and 28 September 2017 resulted in D_{LOS} subsidence of −2 mm at Ventnor Park on 10 October 2017, a delay of 13 days (Figure 10c). These figures suggest that increased cumulative rainfall may be decreasing the delay between rainfall and displacements.

Descending orbit measurements show similar stepped behaviour for D_{LOS} subsidence at Lowtherville Graben (Figure 11b), but D_{LOS} are not as rapid as in the data from the ascending orbit. Between 15 October 2016 and 30 January 2017 a total of 253.2 mm of rain fell, which appears to have triggered a somewhat linear D_{LOS} subsidence of −4.1 mm over 103 days, likely being prolonged due to the intermediate rainfall events. A more complex trend is seen at Ventnor Park (Figure 11c); some stagnant periods can be identified for heave, however are not as prolonged as for the Lowtherville Graben. It is possible the influence of the upper landslide section described in Figure 2b is leading to the non-linearity of measurements (i.e., local subsidence at Ventnor Park arising from rotation along the lower

section combined with heave from the toe of the upper landslide are producing complex results). It can be noted that higher cumulative rainfalls do tend to trigger prolonged displacements, owing to a generation of higher pore pressures within the landslide. This phenomenon was previously observed by Carey et al. [32].

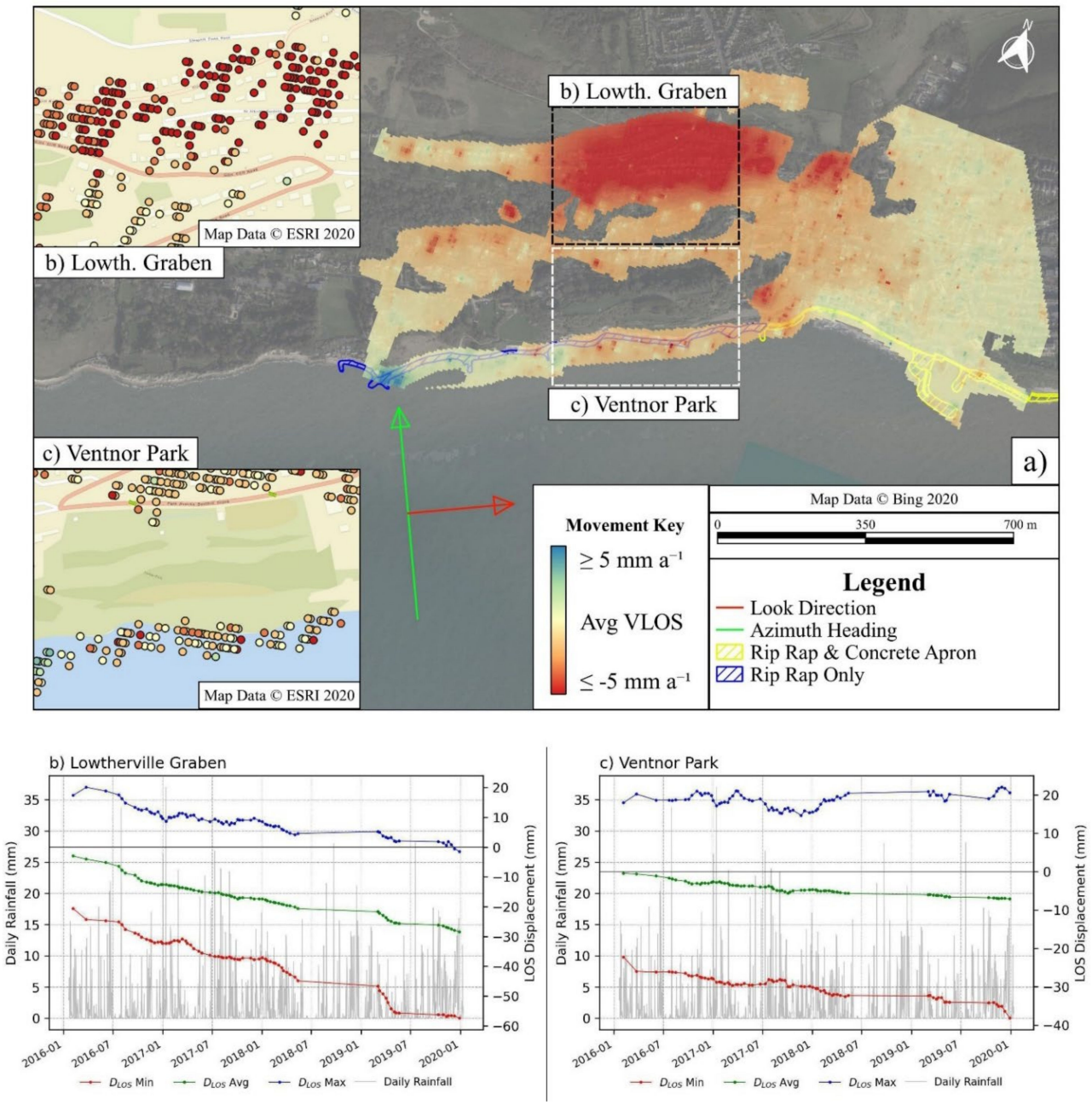


Figure 10. (**a**–**c**): Aerial view of the Ventnor landslide complex IDW of average velocity in mm a^{-1} created from ascending data (Track 132) (**a**). Maximum, average and minimum seven scene moving average D_{LOS} for all selected points shown as insets on (**a**), at the Lowtherville Graben (**b**) and Ventnor Park (**c**). Daily rainfall data from the Ventnor Park rain gauge are also plotted on (**b**,**c**). Image (**a**) was created on QGIS with background imagery from Bing Maps (2020), (**b**,**c**) using background imagery from the ESRI World Street Map (Service Layer Credits: Esri, DeLorme, HERE, USGS, Intermap, iPC, NRCAN, Esri Japan, METI, Esri China (Hong Kong), Esri (Thailand), MapmyIndia, Tomtom).

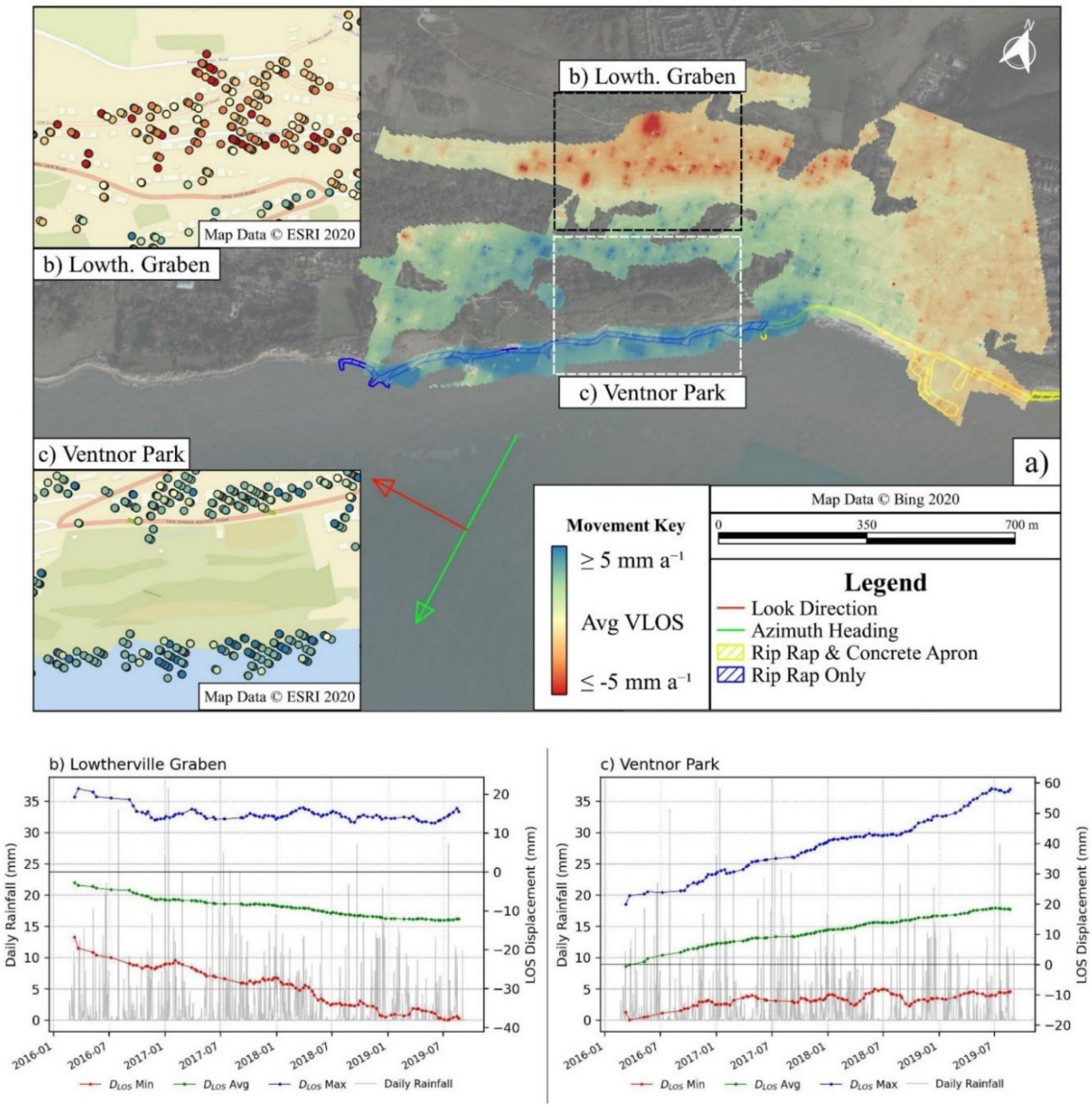


Figure 11. (**a**–**c**): Aerial view of the Ventnor landslide complex IDW of average velocity in mm a^{-1} created from descending data (Track 81) (**a**). Maximum, average and minimum seven scene moving average D_{LOS} for all selected points, shown as insets on (**a**), at the Lowtherville Graben (**b**) and Ventnor Park (**c**). Daily rainfall data from the Ventnor Park rain gauge are also plotted on (**b**,**c**). Image (**a**) created on QGIS with background imagery from Bing Maps (2020), (**b**,**c**) using background imagery from the ESRI World Street Map (Service Layer Credits: Esri, DeLorme, HERE, USGS, Intermap, iPC, NRCAN, Esri Japan, METI, Esri China (Hong Kong), Esri (Thailand), MapmyIndia, Tomtom).

D_{LOS} trends at Lowtherville Graben in ascending and descending orbit data sets, with scatterers moving away from the satellites in both, are consistent with an ongoing rotational landslide predicted by the ground model in Figure 2b. Trends at Ventnor Park, away from the satellite in ascending orbit and toward the descending orbit, follow the observation of an E-W component to the landslide shown in Figure 8b. Similar observations were made in Section 4.2 of Fuhrmann and Garthwaite [42].

The potential effect of coastal defences in the form of a concrete apron fronted by a rip rap extending from Ventnor Beach to Wheeler's Bay further east can be seen qualitatively

from both IDW plots. V_{LOS} observed in areas immediately behind these coastal defences is significantly lower, which compares well with results from Chandler [28]. Defences in the form of rip rap alone are less effective, as seen in the IDW maps presented in Figures 10 and 11. While the exact mechanism of stabilisation was not fully investigated as part of this study, it is likely due to a combination of toe weighting balancing out the sliding mass in the lower section of the landslide. Furthermore, there was toe protection reducing erosion of material along the coastline. The benefit of a greater amount of material being present, behind more heavily protected sections, provides additional sliding resistance. Comparing results from Tables 4 and 5, it is seen that estimates of ground movement rates decrease with a larger data set. This trend is similar to trends in previous monitoring surveys discussed in Section 2.2.

Table 5. Summary of min and max vertical (V_U) and horizontal (V_E) in Ventnor for full time series.

Time Series	Value	V_U (mm a^{-1})	V_E (mm a^{-1})
Full	Min (Subsidence/West)	−9.8	−3.7
	Max (Heave/East)	8.5	12.4

A drawback to the requirement of only using scenes captured within a one-hour buffer of low tide was the significant number of rejected scenes. It is possible that using all scenes and focusing on the inland sections of the slide (i.e., those not affected by tidal cover) would have yielded further information on seasonal ground movement on the upper sections of the landslide. However, the aim of this study was to monitor coastal landslide processes, hence the priority was to generate PS along the coastline.

5. Conclusions

This research presents a case study where PSI was successfully applied to monitor ground movement of an active coastal landslide. While landslide monitoring using InSAR methods was covered in the literature [11–14], no studies to date have focused on coastal landslides, which was the aim of this paper. PSI processing was performed on four years' worth of ascending and descending Sentinel-1 data. Scenes captured at low tide were processed in order to increase the number of PS points identified along coastal defences. While this led to a lower number of observations, it was possible to determine accurate ground movement rates, consistent with ground truth in prior studies.

Significant ground movements are observed in PSI-processed Sentinel-1 across Ventnor, in particular along sections of the coastline that are fronted by coastal defences in the form of a rip rap only. PSI analysis was complemented by historical ground investigation records and monitoring surveys carried out at Ventnor. The combination of PSI results and intrusive boreholes allowed for the development of a new ground model spanning E-W parallel to the coastline, postulating a failure surface at approximately 0 mOD in the Gault Clay, as described in the borehole logs. The failure surface is inclined at 3° to the horizontal, resulting in a significant V_E displacement of approximately 12.4 mm a^{-1} to the east, indicating the overlying block of the landslide complex is displacing more in an easterly direction than vertically (−9.8 mm a^{-1}), while the underlying block remains static. This E-W movement was observed on the section of the coastline protected only by rip rap, whereas ground movements were significantly lower along a section of the coastline further east protected by rip rap and a concrete apron. This shows the value of combined coastal defences as a plausible effective coastal erosion management tool. Qualitatively, the results align well with ground models developed in previous studies of the Ventnor landslide. The benefit of PSI being able to cover large areas over long time periods allows for the visualization of heave at Park Avenue and along the coastline, and subsidence at the Lowtherville Graben and Ventnor Park, following the two tier rotational landslide mechanism previously observed. Similarly, the trend of average ground movement rates decreasing with larger data sets was also observed. The value in analysing non-linear displacement behaviour was assessed previously by Ferretti et al. [43].

Correlation of daily rainfall to spikes in average ground displacement indicated a lag between high rainfall events and large displacements of approximately 13–20 days at Ventnor Park and the Lowtherville Graben, respectively. This correlates with the physical processes observed by Carey et al. [32] as discussed in Section 2.2, however the 29-day delay observed was noticeably longer than the 13–20 days observed in this study. While the physical mechanism of rainfall increasing the landslide movement was not investigated as part of this study, it does follow a similar trend to the process described in Carey et al. [32], where the delay in landslide mechanism was caused by prolonged rainfall and subsequent higher pore pressure generation driving the landslide, resulting in larger peaks.

This study presents a method which can be readily applied for similar monitoring of coastal landslides in urban environments worldwide, even in cases with a dominantly N-S component on movement, as in Ventnor. The complementary approach of combining PSI analysis, historical ground investigations and ground monitoring survey data would be dependent on the availability of records from local and private sources. The use of these direct survey/investigation methods allows for geomorphological interpretation of the PSI results. The result is a cost-effective method available to local authorities, asset managers and designers of coastal defences to monitoring landslides, owing to the open source and continuous nature of InSAR data, and the capability to investigate large areas at ease.

Author Contributions: This article was conceptualised by J.A.L. and G.M.; the methodology, validation and analysis were undertaken by W.O., G.M. and J.A.L.; the software analysis was conducted by S.A. and J.S.; the original draft was prepared by W.O.; reviewing and editing was undertaken by all authors; supervision was conducted by J.A.L., P.J.M. and R.G.; project administration, J.A.L., R.G. and P.J.M. All authors have read and agreed to the published version of the manuscript.

Funding: This research was funded in part by the Engineering and Physical Sciences Research Council (EPSRC), grant number EP/L016826/1 and by Skempton Scholarship.

Institutional Review Board Statement: Not applicable.

Informed Consent Statement: Not applicable.

Conflicts of Interest: The authors declare no conflict of interest.

References

1. Mentaschi, L.; Vousdoukas, M.I.; Pekel, J.; Voukouvalas, E.; Feyen, L. Global long-term observations of coastal erosion and accretion. *Sci. Rep.* **2018**, *8*, 12876. [CrossRef] [PubMed]
2. European Commission. *Living with Coastal Erosion in Europe—Sediment and Space for Sustainability*; European Commission: Brussels, Belgium, 2004; p. 40.
3. Miles, L.; Kingdom, L.; Lightbody, S. Rail Tunnels through Chalk Cliffs: The Importance of Remote Sensing and Geotechnical Mapping in Developing an Understanding of Cliff Regression. In *Engineering in Chalk*; ICE Publishing: London, UK, 2018; pp. 323–330. [CrossRef]
4. Asoni, S.G.; Stavrou, A.; Lawrence, J.A. Developing a GIS Based Methodology for Coastal Chalk Cliff Retreat Using Multiple Datasets. In *Engineering in Chalk*; ICE Publishing: London, UK, 2018; pp. 369–374. [CrossRef]
5. Stavrou, A.; Lawrence, J.A.; Mortimore, R.N.; Murphy, W. A geotechnical and GIS based method for evaluating risk exposition along coastal cliff environments: A case study of the chalk cliffs of southern England. *Nat. Hazards Earth Syst. Sci.* **2011**, *11*, 2997–3011. [CrossRef]
6. Hutchinson, J.N.; Bromhead, E.N. Keynote Paper: Isle of Wight landslides. In *Instability Planning and Management: Seeking Sustainable Solutions to Ground Movement Problems, Proceedings of the International Conference Organised by the Centre for the Coastal Environment, Isle of Wight Council, Ventnor, UK, 20–23 May 2002*; McInnes, R.G., Jakeways, J., Eds.; Thomas Telford: Ventnor, UK, 2002; pp. 3–70.
7. Isle of Wight Council. *Isle of Wight Shoreline Management Plan 2*; Isle of Wight Council: Newport, UK, 2010. Available online: http://www.coastalwight.gov.uk/smp/contents.htm (accessed on 25 May 2020).
8. Liu, J.; Mason, P.J. *Image Processing and GIS for Remote Sensing: Techniques and Applications*, 2nd ed.; Wiley Blackwell: Chichester, UK, 2016; pp. 113–125.
9. Sentinel-1—ESA EO Missions—Earth Online—ESA. Available online: https://earth.esa.int/web/guest/missions/esa-operational-eo-missions/sentinel-1 (accessed on 20 May 2020).

10. Polcari, M.; Albano, M.; Montuori, A.; Bignami, C.; Tolomei, C.; Pezzo, G.; Falcone, S.; La Piana, C.; Doumaz, F.; Salvi, S.; et al. InSAR Monitoring of Italian Coastline Revealing Natural and Anthropogenic Ground Deformation Phenomena and Future Perspectives. *Sustainability* **2018**, *10*, 3152. [CrossRef]
11. Yin, Y.; Zheng, W.; Liu, Y.; Zhang, J.; Li, X. Integration of GPS with InSAR to monitoring of the Jiaju landslide in Sichuan, China. *Landslides* **2010**, *7*, 359–365. [CrossRef]
12. Ciampalini, A.; Raspini, F.; Lagomarsino, D.; Catani, F.; Casagli, N. Landslide susceptibility map refinement using PSInSAR data. *Remote Sens. Environ.* **2016**, *184*, 302–315. [CrossRef]
13. Refice, A.; Spalluto, L.; Bovenga, F.; Fiore, A.; Miccoli, M.; Muzzicato, P.; Nitti, D.; Nutricato, R.; Pasquariello, G. Integration of persistent scatterer interferometry and ground data for landslide monitoring: The Pianello landslide (Bovino, Southern Italy). *Landslides* **2019**, *16*, 447–468. [CrossRef]
14. Aslan, G.; Foumelis, M.; Raucoules, D.; Michele, M.D.; Bernardie, S.; Cakir, Z. Landslide Mapping and Monitoring Using Persistent Scatterer Interferometry (PSI) Technique in the French Alps. *Remote Sens.* **2020**, *12*, 1305. [CrossRef]
15. Holtgrave, A.-K.; Röder, N.; Ackermann, A.; Erasmi, S.; Kleinschmit, B. Comparing Sentinel-1 and -2 Data and Indices for Agricultural Land Use Monitoring. *Remote Sens.* **2020**, *12*, 2919. [CrossRef]
16. Sajinkumar, K.S.; Bincy, H.S.; Bouali, E.H.; Oommen, T.; Vishnu, C.L.; Anilkumar, Y.; Thrivikramji, K.P.; Keerthy, S. Picturing beach erosion and deposition trends using PSInSAR: An example from the non-barred southern west coast of India. *Wetl. Ecol. Manag.* **2020**. [CrossRef]
17. Crosetto, M.; Monserrat, O.; Cuevas-González, M.; Devanthéry, N.; Crippa, B. Persistent scatterer interferometry: A review. *ISPRS J. Photogramm. Remote Sens.* **2016**, *115*, 78–89. [CrossRef]
18. Manconi, A.; Kourkouli, P.; Caduff, R.; Strozzi, T.; Loew, S. Monitoring Surface Deformation over a Failing Rock Slope with the ESA Sentinels: Insights from Moosfluh Instability, Swiss Alps. *Remote Sens.* **2018**, *10*, 672. [CrossRef]
19. Mulas, M.; Corsini, A.; Cuozzo, G.; Callegari, M.; Hiebes, B.; Mair, V. Quantitative Monitoring of Surface Movements on Active Landslides by Multi-Temporal, High-Resolution X-Band SAR Amplitude Information: Preliminary Results. In *Landslides and Engineered Slopes. Experience, Theory and Practice*; CRC Press: Boca Raton, FL, USA, 2016; pp. 1511–1516. [CrossRef]
20. New Maps from Old Photos: Measuring Coastal Erosion—USGS. Available online: https://www.usgs.gov/news/new-maps-old-photos-measuring-coastal-erosion (accessed on 20 May 2021).
21. Shoreline Mapping History. Available online: https://shoreline.noaa.gov/intro/index.html (accessed on 15 July 2020).
22. Jaboyedoff, M.; Oppikofer, T.; Abellán, A.; Derron, M.H.; Loye, A.; Metzger, R.; Pedrazzini, A. Use of LIDAR in landslide investigations: A review. *Nat. Hazards* **2012**, *61*, 1–24. [CrossRef]
23. Mortimore, R. Structural geology of the Upper Cretaceous Chalk Central Mass, Isle of Wight, U.K. *Proc. Geol. Assoc.* **2011**, *122*, 298–331. [CrossRef]
24. British Geological Survey. *Digital Geological Map of Isle of Wight*; BGS: Keyworth, UK, 2013.
25. Borehole Scans. Available online: https://www.bgs.ac.uk/data/boreholescans/home.html (accessed on 10 July 2020).
26. Isle of Wight Council. *Halcrow, Ventnor Undercliff, Isle of Wight Coastal Instability Risk: Interpretative Report and Quantitative Risk Analysis*; Technical report to the Isle of Wight Council; Isle of Wight Council: Newport, UK, 2006.
27. BGS Lexicon of Named Rock Units. Available online: https://www.bgs.ac.uk/lexicon/home.html (accessed on 15 June 2020).
28. Chandler, M.P. The Costal Landslides Forming the Undercliff of the Isle of Wight. Ph.D. Thesis, Imperial College of Science and Technology London, London, UK, 1984.
29. Geomorphological Services Limited (For the Department of the Environment). *Coastal Landslip Potential Assessment: Isle of Wight Undercliff*; Research Contract PECD 7/1/272; Geomorphological Services Limited: Ventnor, UK, 1991.
30. Moore, R.; Carey, J.; McInnes, R.; Houghton, J. Climate change, so what? Implications for ground movement and landslide event frequency in the Ventnor Undercliff, Isle of Wight. In Proceedings of the International Conference Landslides and Climate Change, Ventnor, UK, 21–24 May 2007; McInnes, R.J., Jakeways, J., Fairbank, H., Mathie, E., Eds.; Taylor & Francis: London, UK, 2007; pp. 335–344. [CrossRef]
31. Environment Agency (Romsey District Office). *Daily Rainfall Data for Locations on the Isle of Wight*; Environment Agency: Romsey, UK, 2020.
32. Carey, J.; Moore, R.; Petley, D. Patterns of movement in the Ventnor landslide complex, Isle of Wight, southern England. *Landslides* **2015**, *12*, 1107–1118. [CrossRef]
33. Council Fully Close Newport Road, Ventnor Due to Ground Movement. Available online: https://onthewight.com/council-fully-close-newport-road-due-to-ground-movement/ (accessed on 5 June 2020).
34. Landslip after Wall Collapses in Ventnor. Available online: https://www.bbc.com/news/uk-england-hampshire-51140199 (accessed on 23 May 2020).
35. Family Evacuated After Landslide in Ventnor. Available online: https://www.islandecho.co.uk/family-evacuated-after-landslide-in-ventnor/ (accessed on 10 March 2021).
36. Ferretti, A.; Prati, C.; Rocca, F. Permanent scatterers in SAR interferometry. *IEEE Trans. Geosci. Remote Sens.* **2001**, *39*, 8–20. [CrossRef]
37. Ferretti, A.; Monti-Guarnieri, A.; Prati, C.; Rocca, F.; Massonnet, D. *InSAR Principles: Guidelines for SAR Interferometry Processing and Interpretation*; ESA Publications: Noordwijk, The Netherlands, 2007; pp. B11–B55.
38. ASF Data Search—Vertex. Available online: https://search.asf.alaska.edu/#/ (accessed on 28 May 2020).

39. British Oceanographic Data Centre. *Sea Level Data Portal Data Request—Portsmouth*; British Oceanographic Data Centre: Liverpool, UK, 2020.
40. Mider, G.; Lawrence, J.; Mason, P.; Ghail, R. Monitoring Littoral Platform Downwearing Using Differential SAR Interferometry. *Remote Sens.* **2020**, *12*, 3243. [CrossRef]
41. Raspini, F.; Cigna, F.; Moretti, S. Multi-temporal mapping of land subsidence at basin scale exploiting Persistent Scatterer Interferometry: Case study of Gioia Tauro plain (Italy). *J. Maps* **2012**, *8*, 514–524. [CrossRef]
42. Fuhrmann, T.; Garthwaite, M.C. Resolving Three-Dimensional Surface Motion with InSAR: Constraints from Multi-Geometry Data Fusion. *Remote Sens.* **2019**, *11*, 241. [CrossRef]
43. Ferretti, A.; Prati, C.; Rocca, F. Non-linear subsidence rate estimation using permanent scatterers in differential SAR interferometry. *IEEE Trans. Geosci. Remote Sens.* **2000**, *38*, 2202–2212. [CrossRef]